Tellus (2003), 55B, 723–730
Printed in UK. All rights reserved

TELLUS
ISSN 0280–6509

Large-eddy simulation of double-plume formation induced by CO_2 dissolution in the ocean

By BAIXIN CHEN[1]*, YONGCHEN SONG[1], MASAHIRO NISHIO[2] and MAKOTO AKAI[2], [1]*Research Institute of Innovative Technology for the Earth, Tsukuba-Division of RITE, 1-2-1 Namiki, Tsukuba East, Tsukuba 305-8564, Japan;* [2]*National Institute of Advanced Industrial Science and Technology, 1-2-1 Namiki, Tsukuba East, Tsukuba 305-8564, Japan*

(Manuscript received 2 January 2002; in final form 31 July 2002)

ABSTRACT

Using two-fluid LES technology, a numerical model is developed to simulate double-plume formation under conditions relevant to CO_2 ocean sequestration applications. A small-scale ocean turbulent flow is created and maintained by a forced-dissipative mechanism and LES. Data on ocean currents, temperature and salinity were employed by the model as inlet boundary and initial conditions, respectively. A set of empirical formulae, calibrated with laboratory experimental data, was developed to describe momentum, mass and heat transfer phenomena. Using this model, the influence of the initial diameter of CO_2 droplets released in the deep ocean and thermal effects on the structure of two plumes were investigated. The height of the CO_2 droplet plume and the local minimum pH within the CO_2-enriched seawater plume were found to be very sensitive to the initial diameter of injected CO_2 droplets. Plume height and pH are two key parameters to assess CO_2 sequestration efficiency and related biological impacts. Thermal effects associated with CO_2 dissolution appeared to have limited influence on CO_2-enriched seawater plume structure and pH, but can significantly affect the LCO_2 plume and the temperature field near the CO_2 injection nozzle.

1. Introduction

Two-fluid plumes that develop from the continuous release of one fluid into another and which are driven by buoyancy in density-stratified environments are widely encountered in chemical engineering, deep-sea blowouts of oil or natural gas and in CO_2 ocean sequestration. The last example is an application that has become a topic of interest to environmental scientists during the last decade. CO_2 ocean sequestration is being considered to mitigate rising CO_2 concentrations in the atmosphere. LCO_2 (liquid carbon dioxide) separated from fossil-fuel power-plant exhaust gases can be injected directly into the ocean at depth of about 1000 m (Adams et al., 1997). The buoyant LCO_2 droplets rise and dissolve into surround seawater, releasing heat of solution. The resulting fluid parcels of CO_2-enriched seawater are negatively buoyant. Coupled with the ocean current, droplets interact with pure seawater and with CO_2-enriched seawater to form a separated double plume. Besides the fundamental interest in the physics and chemistry of this flow, studies are required to address a number of practical issues, including how to prevent CO_2 released in the deep ocean from returning to the atmosphere, and how to limit biological impacts. Important insight into those issues is provided by the plume height, which must not intrude into the ocean mixing layer, and by the pH distribution.

To assess the potential of and to develop the technology for CO_2 ocean sequestration, field studies are desirable. However, such experiments are complicated, expensive, and somewhat risky without some prior understanding of the behavior of the plumes formed.

*Corresponding author.
e-mail: b.chen@aist.go.jp

Numerical simulations based on a reasonable model should therefore be conducted in advance of a field experiment.

Development of a viable numerical model of a CO_2 injection plume in the ocean requires understanding of the fundamental dynamics of two-fluid/phase plumes. Such plumes have had been investigated both by laboratory experiments (Socolofsky et al., 2000; Asaeda and Imberger, 1993) and by theoretical analyses (McDougall, 1978). Behavior such as plume separation and peeling has been observed both in stratified and non-stratified environments. Phenomenological flux models have been developed (McDougall, 1978; Liro et al., 1992) that describe overall geometries and key plume parameters, but not the detailed structure of the plume. Alternatively, computational fluid dynamic (CFD) models are being developed (Alendal et al., 1998; Sato and Hama, 2000; Chen et al., 2000) based on two-fluid flow theory and large eddy simulation (LES) technology that provide detailed information on the dynamics and properties of the double plume. These models solve the Navier–Stokes equations for dispersed phase LCO_2 droplets, interacting with continuous-phase ocean water. The CFD models simulate small-scale ocean turbulent flow (ocean domain of several kilometres over times of the order of hours) (Chen et al., 2000) and momentum, mass and energy transfers between LCO_2 droplets and seawater.

In this study, we first extend the model developed by Chen et al. (2000). Recent experimental data are used to refine values of CO_2 droplet drag coefficient, CO_2 solution density, effective Sherwood number and CO_2 solubility in seawater with and without hydrate formation. The model is then used to predict plume behavior during an international field experiment of CO_2 ocean sequestration that is scheduled to be conducted in mid-2002. These numerical simulation results are discussed and summarized.

2. Two-fluid model and fluids exchange sub-models

2.1. Two-fluid model

Since processes occurring near to the CO_2 release point are of primary interest, the computational domain is set up with a space scale of 0 (1.0 km) in both the horizontal and vertical directions. The vertical coordinate is centered at the ocean bottom. LCO_2 droplets are released at a height of H from the ocean bottom. This smaller-scale ocean flow field can be regarded as a horizontal-quasi-homogeneous and vertically stratified turbulent flow. It is well suited for application of the Large-Eddy Simulation method, where the cut-off scale falls within the dissipation wavelength (Woods, 1985; Ledwell et al., 1998).

Assuming a forced-dissipative mechanism of small-scale ocean turbulence (Ledwell et al., 1998) and applying Schumann's filtering technique (Schumann, 1985), the governing equations (for mass, momentum and scalars) for the seawater can be written as:

$$\frac{\partial \overline{\rho}}{\partial t} + \frac{\partial \overline{\rho}\hat{u}_i}{\partial x_i} = \dot{w}_{\mathrm{dco}} \tag{1}$$

$$\frac{\partial \overline{\rho}\hat{u}_i}{\partial t} + \frac{\partial \overline{\rho}\hat{u}_i\hat{u}_j}{\partial x_j} = -\frac{\partial \hat{p}}{\partial x_i} + \frac{\partial \overline{\rho}\hat{\tau}_{ij}}{\partial x_j} + (\overline{\rho} - \rho_o)g_i + F_{tF}\delta_{ij} + (\dot{F}_{\mathrm{dco}}) \tag{2}$$

$$\frac{\partial \overline{\rho}\hat{\varphi}}{\partial t} + \frac{\partial \overline{\rho}\hat{\varphi}\hat{u}_j}{\partial x_j} = \frac{\partial}{\partial x_j}\left(\overline{\rho} D_\varphi \frac{\partial \hat{\varphi}}{\partial x_j}\right) + \frac{\partial \overline{\rho}\hat{q}_\varphi}{\partial x_j} + \dot{S}\varphi \tag{3}$$

in which resolved variables, (^), include the velocity vector, $\hat{u}_i$; dynamic pressure, $\hat{p}$, defined by the hydrostatic pressure and initial density, ρ_0; and scalars, $\hat{\varphi}$, including temperature, salinity and mass fraction of dissolved CO_2. The scalar variables are used to calculate pure seawater density, ρ_s, using the equation of state for seawater (Unesco, 1981), and CO_2–seawater solution density, ρ_w, using an empirical equation determined from laser interferometer experiments by the authors (Song et al., 2001):

$$\rho_w = \rho_s(1.0 + 0.275\chi) \tag{4}$$

here χ is the CO_2 mass fraction in CO_2-enriched seawater. $\overline{\rho} = (1.0 - \alpha)\rho_w$, where α is the void fraction of LCO_2 droplets that is defined below. Expressions for source terms arising from interactions between the two fluids [i.e. the last terms on the RHS of eqs. (1)–(3)], will be provided in the next section.

The above system is forced at lower-frequency mode across a narrow wavenumber band, in two dimensions, in horizontal momentum equations for seawater by a turbulent force, F_{tF}, when $\delta_{11} = \delta_{22} = 1$. This turbulent force is generated and controlled by Markovian processes and expressed as:

$$F_{tF}(t) = sign(Rnd - 0.5)(1 - \beta^2)^{1/2} u_0' \xi(z) e^{(-6K_c^2)} + \beta F_{tF}(t - \Delta t) \tag{5}$$

where β is a forcing time scale and *Rnd* a random number from 0 to 1. The lower-frequency mode parameter, K_c, is determined by $K_c \leq 0.06|Rnd - 0.5|$. The r.m.s. velocity, u'_0, is a forcing intensity variable and $\xi(z)$ is a non-dimensional mean velocity distribution function in the vertical direction that is determined by experiment data.

The turbulent dissipation and transport terms, $\hat{\tau}_{ij}$ and $\hat{q}_\varphi$, in sub-grid scale are estimated by means of a structure function model (Lesieur, 1996) independently in the horizontal and vertical directions. A detailed discussion of small-scale turbulent simulation can be found in (Chen et al., 2000).

Since the simulation must account for a large quantity of LCO_2 being injected continuously, an Eulerian–Eulerian two-fluid frame (Sirignano, 1986) is adopted to describe the dynamics of the LCO_2 plume under the memory limitations of present-generation computers. As a quasi-fluid, the continuum equation for LCO_2 droplets is decomposed into two equations for droplet void fraction, α, and number density, f, in order to estimate diameter shrinkage resulting from droplet dissolution. For simplicity, we assume droplet coalescence, secondary break-up and collisions have negligible effect on the number density function, f, when a hydrate film covers the droplets. The governing equations of the LCO_2 fluid can then be derived that satisfy the LES concept of cut-off fitting:

$$\frac{\partial \hat{f}}{\partial t} + \frac{\partial \hat{f}\hat{u}_{dj}}{\partial x_j} = 0 \tag{6}$$

$$\frac{\partial \hat{\alpha}}{\partial t} + \frac{\partial \hat{\alpha}\hat{u}_{\mathrm{d}j}}{\partial x_j} = -\dot{w}_{\mathrm{dco}}/\rho_{\mathrm{d}} \tag{7}$$

$$\frac{\partial \overline{\rho}_{\mathrm{d}}\hat{u}_{\mathrm{d}i}}{\partial t} + \frac{\partial \rho_{\mathrm{d}}\hat{u}_{\mathrm{d}i}\hat{u}_{\mathrm{d}j}}{\partial x_j} = \frac{\partial \overline{\rho}_{\mathrm{d}}\hat{\tau}_{\mathrm{d}ij}}{\partial x_j} + \hat{\alpha}(\rho_{\mathrm{d}} - \rho_{\mathrm{w}})g_i - (\dot{F}_{\mathrm{dco}})_i \tag{8}$$

where the subscript "d" denotes LCO_2 droplet and $\overline{\rho}_{\mathrm{d}} = \hat{\alpha}\rho_{\mathrm{d}}$, where the droplet density is a constant. The turbulent transport terms for this quasi-fluid are closed by a sub-grid scale (SGS) model (Ferziger, 1993) based on the droplet field. The cross-coupling between the ocean turbulent flow and droplets is represented by the exchange source terms, which are introduced below.

2.2. Fluid exchange terms

LCO_2 droplets might be modeled using empirical formulations that can be found in the technical literature (e.g. Clift et al., 1978). It has been observed (Ozaki, 1999), however, that a hydrate film on the surface of LCO_2 droplet can lead to behavior that deviates from that of liquid-only droplets. To account for this, a new set of sub-models for mass, momentum and heat transfer between LCO_2 droplets and seawater was developed. The fundamental assumption, based on experimental observations (as shown in Fig. 1), is that a CO_2 droplet, under conditions where a hydrate film can form, must be regarded as a rigid irregular-ellipse particle with permeable and immersable surface. The rigid irregular ellipse is the description of droplet geometry, and the permeable and immerseable surface allows mass transfer at the interface between CO_2 droplets and seawater.

For momentum exchange, the source term can be expressed as:

$$\dot{F}_{\mathrm{dco}j} = 0.75(\pi/6)^{1/3}\rho_{\mathrm{d}}\nu_{\mathrm{w}}\hat{\alpha}^{2/3}\hat{f}^{1/3}C_{\mathrm{dd}}|\hat{u}_{\mathrm{j}} - \hat{u}_{\mathrm{d}j}|(\hat{u}_j - \hat{u}_{\mathrm{d}j}) \tag{9}$$

where ν_{w} is the kinematic viscosity of seawater.

Because of deformation, the effective projected area of a CO_2 droplet, A_{eff}, is larger than that of a sphere, A_{eq}, with the same volume. This larger projected area enhances the drag force on the droplet. The effective drag coefficient, C_{dd}, is then defined as a function of Reynolds number, *Re*, and is modified by taking the deformation [the ratio of projected areas $(A_{\mathrm{eff}}/A_{\mathrm{eq}})_{\mathrm{p}}$] into account:

$$C_{\mathrm{dd}} = 24(1.0 + 0.125Re^{0.72})(A_{\mathrm{eff}}/A_{\mathrm{eq}})_{\mathrm{p}}Re^{-1} \tag{10}$$

$$(A_{\mathrm{eff}}/A_{\mathrm{eq}})_{\mathrm{p}} = 1.0 + Re(5.6419 - 8.3484 \times 10^{-3}Re + 1.4596 \times 10^{-5}Re^2) \times 10^{-4} \tag{11}$$

where *Re* is calculated using slip velocity, droplet equivalent diameter and the kinematic viscosity of seawater.

Terminal velocities calculated using eqs. (10) and (11) are compared with experimental data as shown in Fig. 2. Calculations agreed well with experimental data for three different seawater conditions. The figure also includes terminal velocities calculated using the rigid-sphere drag coefficient, C_{d}. Those velocities are much higher than the data, especially for large droplets. This implies that LCO_2 plume height may be over predicted if droplet deformation is not considered in the numerical simulations.

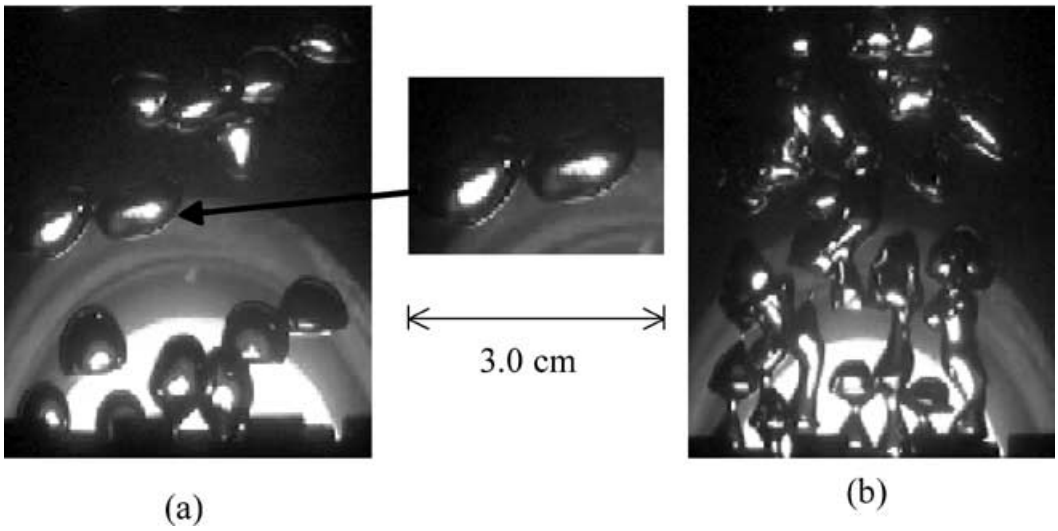

Fig. 1. Experimental observation of CO_2 droplet rising and deformation (Ozaki, 1999): (a) mono-dispersed droplets; (b) poly-dispersed droplets.

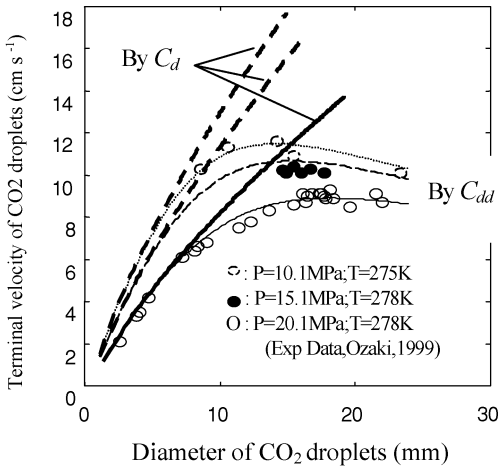

Fig. 2. Comparision on CO_2 droplet terminal velocities with and without deformation, calculation and experimental data (Ozaki, 1999).

Droplet shrinking, or mass transfer, rate can be calculated by:

$$\dot{w}_{\mathrm{dco}} = \pi D_{\mathrm{c}} d_{\mathrm{c}} (C_{\mathrm{s}} - C) Sh_{\mathrm{eff}} \tag{12}$$

where D_c, d_c, C, C_s, and Sh_{eff} are the CO_2 diffusion coefficient in seawater, droplet diameter, CO_2 concentration, CO_2 solubility and effective Sherwood number, respectively. The last two parameters need to be determined empirically.

From experimental data (Ozaki, 1999; Kimuro et al., 1994; Stewart and Munjal, 1970), expressions were found for the effective Sherwood number and CO_2 solubility in seawater that were applied to model mass transfer. By taking the effect of deformation on mass transfer, the effective Sherwood number is expressed as:

$$Sh_{\mathrm{eff}} = (2 + 0.69 Re^{1/2} Sc^{1/3})(A_{\mathrm{eff}}/A_{\mathrm{eq}})_{\mathrm{tot}} \tag{13}$$

$$(A_{\mathrm{eff}}/A_{\mathrm{eq}})_{\mathrm{tot}} = 1.0 + Re(4.6707 - 1.1871 \times 10^{-2} Re + 1.4766 \times 10^{-5} Re^2) \times 10^{-4}. \tag{14}$$

In eq. (14), $(A_{eff}/A_{eq})_{tot}$ is the ratio of total effective droplet area to total area of an equivalent sphere.

CO_2 solubility in seawater, χ_s, as a function of pressure and temperature is estimated from curvefits to experimental data (Kimuro et al., 1994; Stewart and Munjal, 1970). As indicated by Aya et al. (1997), CO_2 solubility decreases with decreasing temperature in the hydrate formation regime (temperature lower than the critical temperature T_f), but increases with decreasing temperature in the hydrate-free regime. These properties are modeled separately in this study. For the hydrate formation regime, a normalized expression for CO_2 solubility is:

Table 1. *Coefficients* D_{ij} *in eq. (16) for gas–hydrate (top) and for liquid–hydrate (bottom)*

Gas-hydrate

$(P/p_r \le 1)$	$J=0$	$J=1$	$J=2$	$J=3$
$I=1$	−0.047 10	−0.054 90	−0.3103	0.0
$I=2$	0.315 20	−1.225 10	0.8483	0.0

Liquid-hydrate

$(P/p_r > 1)$	$J=0$	$J=1$	$J=2$	$J=3$
$I=1$	−0.3245	−0.1747	0.1119	−0.024 10
$I=2$	−0.1892	0.2195	−0.1249	0.028 10

$$\frac{\chi_s}{\chi_f} = 1.0 + \sum_{i=1}^{2} C_i[(T_f - T)/(T_r - T_{ref})]^i \tag{15}$$

$$C_i = \sum_{j=0}^{3} D_{ij} p_k^j \tag{16}$$

where $T_{ref} = -0.753 \times 10^{-2} p$ (p in MPa; T in °C); $P_k = P/p_r$; and the coefficients D_{ij} are listed in Table 1 for gas–hydrate ($P/p_r \le 1$, top) and for liquid–hydrate ($P/p_r > 1$, bottom); respectively.

To distinguish the states between hydrate and liquid/gas, we need to determine the relationship between CO_2 solubility and the critical temperature, T_f, which itself is a monotropic function of pressure. This critical solubility can be expressed as:

$$\chi_f = \sum_{i=0}^{3} B_i (T_f/T_r)^i \tag{17}$$

$$T_f/T_r = 1.0 + \sum_{i=1}^{3} A_i (p/p_r - 1.0)^i \tag{18}$$

where the coefficients B_i and A_i are listed in Tables 2 and 3 and $p_r = 4.1983$ MPa, $T_r = 8.7156$ °C for seawater.

Table 2. *Coefficients* B_i *in eq. (17)*

	B_0	B_1	B_2	B_3
$P/p_r \le 1$	0.027 887	0.030 608	−0.022 202	0.020 510
$P/p_r > 1$	−60.3323	178.359	−175.634	57.6640

Table 3. *Coefficients* A_i *in eq. (18)*

	A_1	A_2	A_3
$P/p_r \le 1$	0.807 10	−0.890 30	0.0
$P/p_r > 1$	0.030 70	−0.001 03	0.0

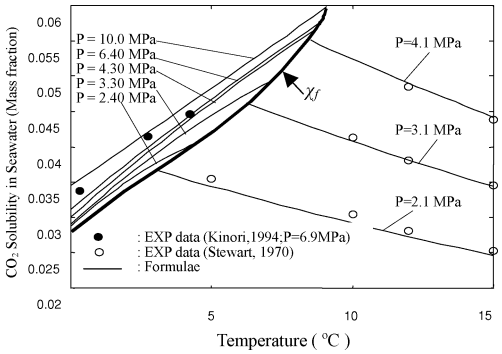

Fig. 3. CO_2 solubility in seawater, model prediction and experimental data (Kemori et al., 1994; Steward and Munjal, 1970).

For the hydrate-free case, CO_2 solubility can be computed by:

$$\begin{aligned}\chi_s = {} & [0.866\,88 + 6.5057 P_k \\ & - (0.3068 + 0.1887 P_k)(T/T_r) \\ & + (0.5266 \times 10^{-3} + 0.1600 P_k) \\ & \times 10^{-2}(T/T_r)^2] \times 10^{-1}.\end{aligned} \tag{19}$$

CO_2 solubility estimated from the sub-models developed in this study [eqs. (15)–(19)] is compared with experimental data in Fig. 3. Critical solubility occurs at the boundary between the gas/liquid CO_2 and hydrate regimes. Below the critical temperature, T_f, solubility decreases with decreasing temperature; above T_f, solubility decreases with increasing temperature. Equations (15)–(19) apply for pressures lower than 12.0 MPa and for temperatures ranging from 0.0 to 20.0 °C.

Regarding heat transfer, it is not prohibitively difficult to predict energy transfers for the hydrate-free case due to CO_2 dissolution, provided that the enthalpy of solution is known. A hydrate film at the CO_2–seawater interface greatly complicates the analysis. The mechanisms of hydrate formation and dissociation at phase interfaces are not well understood, although models are being developed (Mori and Mochizuki, 1997). In this study, based on experimental observations, it is assumed that CO_2 droplets are covered with a thin hydrate film after being injected into the ocean. Furthermore, it is assumed that the thickness of the hydrate film is constant, implying that hydrate formation and dissolution are in quasi-equilibrium, proceeding at similar rates. Under these assumptions,

the heat transport term in the energy equation for seawater is:

$$\dot{S}_t = \dot{w}_{dco}\Delta H_s\left(\frac{\rho_h}{\rho_d}\frac{\Delta H_h}{\Delta H_s}\frac{\dot{V}_h}{\dot{V}_s}\delta(x) + 1.0\right) \quad (20)$$

where $\rho_h = 1.095$ g cm^{-3} is the hydrate density (Aya et al., 1997); $\delta(x = x_{inj}) = 1$ and $\delta(x \neq x_{inj}) = 0$, where x_{inj} is the location of the injection nozzles and $\dot{V}_h$ and $\dot{V}_s$ are the volume-shrinkage rates of the hydrate film and LCO_2 droplet, respectively. The ratio of those two shrinkage rates are modeled as:

$$\frac{\dot{V}_h}{\dot{V}_s} = 1.0 - \left(1.0 - \frac{\delta}{d_c}\right)^2\left(1.0 - 2.0\frac{\delta}{d_c}\right) \quad (21)$$

$$\frac{\delta}{d_c} = C_h\frac{1.0 - (1+n)\chi_s}{(\chi_s - \chi)Sh_{eff}}. \quad (22)$$

$C_h = 0.524 \times 10^{-2}$–$0.524 \times 10^{-1}$ (Mori and Mochizuki, 1997); δ is the thickness of the hydrate film; and n is a parameter known as the hydration number and chosen to be $n = 7.3$. Data obtained by Aya et al. (1997) for CO_2 hydrate formation enthalpy and CO_2 enthalpy of solution were employed in this model. The values are $\Delta H_h = 200.73$ kJ kg^{-1} and $\Delta H_s = 180.7$ kJ kg^{-1}. CO_2 solubility can be determined by eq. (15), and the mass fraction of CO_2 in the surrounding seawater, χ, is calculated by numerically solving eq. (3).

The two sets of equations, eqs. (1)–(8), closed by the sub-models of exchange terms and turbulent models for the dispersed and continuous phases discussed above, were numerically solved and coupled with each other by a finite-volume method in a staggered grid system. Discretization of the momentum equations, eqs. (2) and (8), were accomplished by a second-order central-difference scheme. The scalar equations employed a hybrid scheme comprising fourth-order central plus power-law to limit numerical diffusion and to prevent the errors associated with numerical oscillations. The unsteady terms were approximated by an implicit three-level second-order scheme and the SIMPLEC algorithm was applied to solve the momentum equation.

3. Numerical experiments

The dimensions of the simulation domain were $140 \times 140 \times 200$ (m). A $64 \times 64 \times 128$ grid was employed. Data on deep ocean currents (maximum velocity 3.0 cm s^{-1}) were applied as inlet boundary conditions. The outlet sides of the domain were treated as open boundaries. The top of the domain is a free surface and, for both fluids, was treated as a rigid slip wall according to the investigation of Lam and Banerjee (1996). This is a reasonable and simple approach when no mass transfer is assumed at the top. The bottom of the domain was considered to be a no-slip boundary for velocity vectors and a solid wall for scalars. The CO_2 release rate was 1.0 kg s^{-1} with initial droplet diameters of 8.0 mm (case A) and 5.0 mm (case B). Release occurs at a height of 2 m above the ocean bottom. The simulation was performed as follows: seawater flow is initiated to generate a turbulent fluid field. This small-scale ocean turbulent flow field was maintained by a forced-dissipative mechanism and LCO_2 injection is initiated. The droplet equations are solved to obtain new source terms that couple with the ocean flow field. This computational cycle was terminated and begun again at the next time step when the density difference between cycles fell below a selected threshold.

Figure 4 shows the simulated double-plume structure for cases A and B 60 min after the start of CO_2 injection. The contours corresponded to LCO_2 droplet diameter, and the gradients show the distribution of pH due to droplet dissolution on the central vertical plan of the domain. The left edge of the figure (also in Fig. 5) is the boundary where fresh seawater enters the computation domain. Temperature decreases with depth. The simulations indicated that for 8.0 mm initial diameter droplets, the plume heights (LCO_2 and pH plumes) are 156 m and the lowest pH is 6.5. For smaller 5.0 mm diameter droplets, the plume height is 83 m and the minimum pH is 6.0.

Larger droplets have higher terminal velocities (Fig. 2) and take more time to dissolve seawater completely, which leads to a taller plume. From the point of view of mass transfer, however, a larger initial diameter means that a smaller interface is created, which impedes mass transfer and reduces dissolution rates. This leads to a higher pH and an unremarkable interaction between the LCO_2 plume and CO_2-enriched seawater plume because of the smaller negative buoyancy (compare the two LCO_2 plumes shown in Fig. 4).

To assess energy transfer effects on the plume and temperature field, a case was run at the same conditions as case B but without heat release. Results are plotted in Fig. 4(c). pH distribution and plume structure do not appear to be influenced significantly,

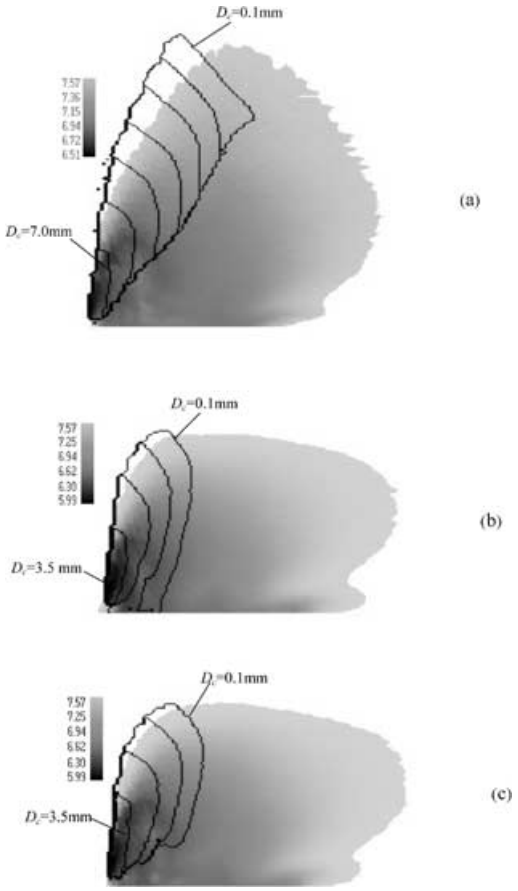

Fig. 4. Double plumes induced by CO_2 ocean sequestration (contours of CO_2 droplet diameter show LCO_2 plume and the image of pH show the CO_2 enriched-seawater plume) plume: (a) case A, (b) case B and (c) case B without heat release.

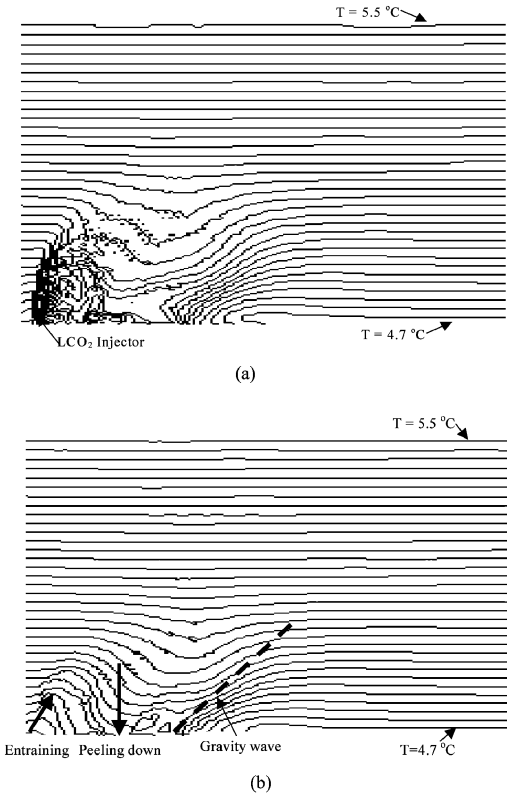

Fig. 5. Temperature field predicted by the model: (a) case B and (b) case B without heat release.

with the exception that the LCO_2 plume near the injection nozzle displays a displacement of droplets toward the bottom. This phenomenon might be explained with the aid of calculated temperature fields shown in Fig. 5; part (a) shows temperature contours for case B (with heat release). While Fig. 5(b) shows temperature field with no heat release. When heat is released by dissolution of CO_2, seawater, especially near the injection nozzles, rises up and enhances the ascent of droplets against the drag from the CO_2–seawater solution. This results in less deformation of the LCO_2 plume outline. For the case of no heat release, the relative velocity seems to be negative downstream of the LCO_2 plume without support from the buoyant seawater.

On the other hand, without heat release, temperature contours can also trace the movement of seawater elements as well as velocity streamlines of fluid. Phenomena observed in laboratory experiments, such as ambient fluid entraining and peeling, is therefore apparent in these results. Upstream of the LCO_2 plume [Fig. 5(b)] seawater is entrained into the plume and then peels down (downstream) due to negative buoyancy arising from the dissolution of CO_2. This flow produces a gravity wave.

4. Conclusions

In this study, a two-fluid LES model of CO_2 ocean sequestration (Chen et al., 2000) was further developed to treat the transport dynamics between LCO_2 and seawater for cases with and without hydrate formation. Sub-models for effective drag coefficient, effective Sherwood number and CO_2 solubility can be

conveniently implemented into a numerical code. The preliminary simulation experiments on CO_2 ocean sequestration predict that the initial droplet diameter is a sensitive parameter for both physical and biological impacts on the ocean. Heat release associated with hydrate formation and CO_2 dissolution seems to have negligible influence on plume structure, except near to the injection nozzle. Seawater entrainment and peeling out of the plume, and gravity waves, were predicted by the model.

5. Acknowledgments

This study is a part of the investigation of the CO_2 Ocean Sequestration Project managed by Research Institute of Innovative Technology for the Earth (RITE) and funded by New Energy and Industrial Technology Development Organization (NEDO), Japan. The authors are grateful to Dr. S.M. Masutani, University of Hawaii, for useful comments and help to improve the paper.

REFERENCES

Adams, E. E., Caulfield, J. A., Herzog, H. J. and Auerbach, D. I., 1997. Impacts of reduced pH from ocean CO_2 disposal: sensitivity of zooplankton mortality to model parameters. *Waste Management* **17**, 275–380.

Alendal, G., Drange, H. and Thorkildsen, F. 1998. Two-phase modeling of CO_2 droplet plumes. NERSC Technical Report, No. 153, 1–33.

Aseada, T. and Imgerger, J. 1993. Structure of bubble plumes in linearly stratification environments. *J. Fluid Mech*. **294**, 35–57

Aya, I., Yamane, K. and Nariai, H. 1997. Solubility of CO_2 and density of CO_2 hydrate at 30 MPa, *Energy* **22**, 263–271,

Chen, B., Masuda, S., Nishio, M., Someya, S. and Akai, M. 2000. Two-fluid turbulent modeling of liquid CO_2 dissolution in the ocean by LES, *Proc. ASME*. FEDSM 2000-11131.

Clift, R., Grace, J. R. and Weber, M. E. 1978. *Bubbles, droplets, and particles*. Academic Press, New York.

Ferziger, J. H. 1993. *Subgrid-scale modeling. Large eddy simulation of complex engineering and geophysical flows*. (Eds. B. Galperin and S. A. Orszag), Combridge University Press.

Kimuro, H., Kusayanagi, T. and Morishita, M. 1994. Basic experimental results of liquid CO_2 injection into the deep ocean. *IEEE Trans. Energy Conversion*, **9**, 732–735.

Lam, K. and Banerjee, S. 1992. On the condition of streak formation in a bounded turbulent flow. *Phys. Fluids A* **4**, 306–320.

Ledwell, J. R., Watson, A. J. and Law, C. S. 1998. Mixing of a tracer in the pycnocline. *J. Geophysi. Rese.* **103**, 21 499–21 529.

Lesieur, M. and Métais, O. 1996. New trends in large-eddy simulations of turbulence. *Annu. Rev. Fluid Mech*. **28**, 45–82.

Liro, C. R., Adams, E. E. and Herzog, H. J. 1992. Modeling the release of CO2 in the deep ocean. *Energy Conserv. Mgmt*. **33**, 667–674.

McDougall, T. J. 1978. Bubble plumes in stratified environments. *J. Fluid Mech.* **85**, 655–672.

Mori, Y. H. and Mochizuki, T. 1997. Mass transport across clathrate hydrate films – a capillary permeation model. *Chem. Eng. Sci.* **52**, 3613–3616.

Ozaki, M. 1999. *Annual Report of RITE 1999*, 286–307 (in Japanese).

Sato, T. and Hama, T. 2000. Numerical simulation of LCO_2 droplet plume in the deep ocean. *Proc. ASME*. FEDSM2000-11149, 1–7

Schumann, U. 1985. Algorithms for direct numerical simulation of shearing-periodic turbulence. *In: Proc. 9th Intl Conf. on Numerical Meth. in Fluid Dynam.* (ed? Soubbaramayer and J. P. Boujot). Lecture Notes in Physics, vol. 218, Springer, Barlin, 492–546.

Sirignano, W. A. 1986. The formulation of spray combustion models' resolution compared to droplet spacing. *ASME J. Heat Transfer* **108**, 633–639.

Stewart, P. and Munjal, P. 1970. Solubility of carbon dioxide in pure water, synthetic sea water, and synthetic sea water concentrations at -5 to 25°C and 10 to 45 atm pressure. *J. Chem. Eng. Data*, **15**, No. 1.

Socolofsky, S. A. 2001. Laboratory experiments of multiphase plumes in stratification and crossflow. Ph.D Thesis, Dept. Civil & Environ. Eng., MIT, Combridge, MA.

Woods, J. 1985. The world ocean circulation experiment. *Nature* **314**, 501–511.

Unesco. 1981. Tenth Report of the Joint Panel on Oceanographic Tables and Standards. Unesco Technical Papers in Marine Science, No. 36, 24–29.

Song, Y., Chen, B. and Nishio, M. 2001. Annual Report of RITE 2001, 63–77 (in Japanese).